Proceedings of the ASME 2020 39th International Conference on Ocean, Offshore and Arctic Engineering
OMAE2020
August 3-7, 2020, Virtual, Online

OMAE2020-18160

REPRESENTATION OF BREAKING WAVE KINEMATICS IN THE FULLY NONLINEAR POTENTIAL FLOW MODEL REEF3D::FNPF

Csaba Pakozdi*
SINTEF Ocean, P.O.Box 4762 Sluppen
N-7465 Trondheim, Norway
Phone: +47 45 42 77 83
Email: csaba.pakozdi@sintef.no

Arun Kamath
Weizhi Wang
Hans Bihs
Dept. of Civil and Env. Eng. NTNU
Trondheim, Norway

ABSTRACT

Robust simulations over three-hours are essential to represent a stationary sea state and derive wave statistics and structural response of marine structures in a reliable manner. This means that the numerical model used for the simulation of the sea state should be computationally efficient, stable and accurate. The fully nonlinear potential flow (FNPF) model solving the Laplace equations is found to be a good tool for this application. The drawback of using the FNPF model is the representation of wave breaking. Due to the assumptions of irrotational flow, it is not possible to represent an overturning free surface which occurs as a result of wave breaking. Therefore, there is a need to investigate a method to represent the effect of wave breaking in an efficient yet accurate manner. In this paper, the open-source model REEF3D::FNPF is used. The model demonstrates good robust performance and stability even in the presence of breaking waves in the domain. However, it is noticed that the free surface in the aftermath of wave breaking is slightly over predicted. This results in waves in the post-breaking region that are higher and steeper than expected after wave breaking. This difference can be avoided by incorporating techniques to correctly reduce the wave energy in the post-breaking region by the means of a reasonable damping mechanism.

Breaking waves generated in the facility at SINTEF Ocean/NTNU are simulated in REEF3D::FNPF. Earlier presented results of Star-CCM+ [1] are used in the comparison. The free surface measured at several different locations in the Small towing tank are compared to the numerical results. As published earlier, the CFD model represents the model test data well. Further, the effect of wave breaking in the numerical models is investigated by comparing the numerical results from both models. The difference in the free surface representation is used to analyze the damping factor required in the FNPF model, compared to the wave kinematics represented in the CFD model. Further, REEF3D::FNPF is used to carry out three-hour long simulations with the JONSWAP spectrum in intermediate water depth conditions in order to identify the influence of the breaking model parameters on the statistical properties of the generated waves and compared against model test data.

INTRODUCTION

The breaking wave impact force significantly influences the design and limit-state analysis of column based offshore structures. The simulation of such extreme breaking waves is not possible using potential theory based models. A unique computational strategy solving the Reynolds-Averaged Navier-Stokes Equations (RANSE) with a two-phase fluid model such as the volume of fluid (VOF) method [2] or the level-set method [3] appears to be the optimal framework able to provide a global modeling of free-surface viscous flows integrating nonlinearities such as the breaking phenomena and turbulence. The literature on the numerical modeling of breaking waves using these tech-

*Address all correspondence to this author.

niques is very large. However, these methods are not practical for efficiently simulating a three-hour stationary sea state due to the enormous computational cost and time. The solution which has begun to become an industrial application, is the coupling of potential theory-based numerical wave tanks (NWT) with a two-phase CFD model [4, 5]. The application area of such numerical wave tanks is only meaningful for steep and high sea states, which cannot be described by analytical models such as second order irregular wave models [6], [7]. The appearance of breaking waves in such sea states of three-hours duration is unavoidable. This means that the NWT simulation crashes when waves starting to break without any strategy to stabilize the potential theory model. One possible solution is using a two-phase CFD simulation immediately before wave breaking, which is technically possible as shown in [8], if only one wave event is of interest in the simulation. In such a coupled method, the waves are propagate a long distance in the NWT and the objective in the simulation is not to simulate each breaking wave properly during propagation but to let the potential theory based simulation survive such an event and mimic the energy dissipation due to the wave breaking. Several techniques are presented in the recent years [4] . The common properties of such techniques is that they are dependent on several numerical coefficients which are defined empirically. This makes it difficult for a user to set up such a NWT simulation.

The objective of this study to identify the parameters of the breaking wave in the potential flow model which closely reproduces the observed energy dissipation due to breaking in a model test for one deterministic wave breaking event. The second objective is to answer the question if one can use only one breaking event to identify these coefficients for a three-hours simulation by identifying the effect of the variation of these parameters with respect to the statistical properties such as power spectrum, the probability of exceedance of the wave crest height as well as the elevation rise velocity at a point in space.

In this paper, the open-source hydrodynamic model REEF3D::FNPF is used to carry out the breaking wave simulation as well as the three-hour long simulations with the JONSWAP spectrum in intermediate water depth conditions. The new numerical wave model FNPF of REEF3D solves the Laplace equation for the flow potential and the nonlinear kinematic and dynamic free surface boundary conditions [9]. Very promising results are seen for the reproduction of the experimental regular and bi-chromatics waves over a constant water depth as well as with complex bottom topography. Results have been presented using this model in [10] and [11]. This approach requires reduced computational resources compared to CFD based NWTs. The REEF3D::FNPF module can use the already implemented functionality of REEF3D [12], where solid boundaries are incorporated through a ghost cell immersed boundary method. Therefore it is capable of simulating wave-structure interaction such as complex sea bottom topography by solving the non-linear potential theory problem. The Laplace equation together with the enclosure of the boundary conditions are solved with a finite difference method on a stretched σ-coordinate system similar to OceanWave3D [13].

Focused breaking waves are generated in the facility at SINTEF Ocean/NTNU and the free surface elevation is recorded at several locations. This model test is simulated by REEF3D::FNPF and as earlier presented by Star-CCM+ [1]. The free surface measured at several different locations in the tank are compared to the numerical results. As in previous publications, the CFD model represents the model test data well. Further, the effect of wave breaking in the numerical model is investigated by comparing the numerical results from both models. The difference in the free surface representation is used to analyze the damping factor required in the FNPF model, compared to the wave kinematics represented in the CFD model.

Statistical properties of the free surface elevation in the numerical wave tank are validated using the available data from model tests carried out at SINTEF Ocean/NTNU in the same facility but with constant water depth and with a different wave maker.

IMPLEMENTATION

As mentioned in the introduction, the governing equation for the fully nonlinear potential flow model in REEF3D::FNPF is the Laplace equation:

$$\frac{\partial^2\Phi}{\partial x^2}+\frac{\partial^2\Phi}{\partial y^2}+\frac{\partial^2\Phi}{\partial z^2}=0. \tag{1}$$

Boundary conditions are required in order to find the unique solution of the velocity potential Φ from this elliptic equation, especially at the free surface and at the seabed. These are the kinematic and dynamic boundary conditions which must be fulfilled at all times and are prescribed as follows:

$$\frac{\partial\eta}{\partial t}=-\frac{\partial\eta}{\partial x}\frac{\partial\widetilde{\Phi}}{\partial x}-\frac{\partial\eta}{\partial y}\frac{\partial\widetilde{\Phi}}{\partial y}+\widetilde{w}\left(1+\left(\frac{\partial\eta}{\partial x}\right)^2+\left(\frac{\partial\eta}{\partial y}\right)^2\right) \tag{2}$$

$$\frac{\partial\widetilde{\Phi}}{\partial t}=-\frac{1}{2}\left|\left(\frac{\partial\widetilde{\Phi}}{\partial x}\right)^2+\left(\frac{\partial\widetilde{\Phi}}{\partial y}\right)^2-\widetilde{w}^2\left(1+\left(\frac{\partial\eta}{\partial x}\right)^2+\left(\frac{\partial\eta}{\partial y}\right)^2\right)\right|-g\eta \tag{3}$$

where η is the free surface elevation, $\widetilde{\Phi}=\Phi(\mathbf{x},\eta,t)$ is the velocity potential at the free surface, $\mathbf{x}=(x,y)$ represents the location

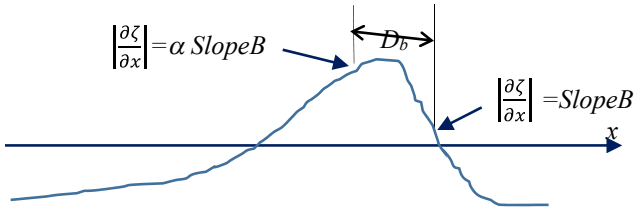

FIGURE 1: Schematic sketch for breaking-wave model definition from [4]

at the horizontal plane and $\widetilde{w}$ is the vertical velocity at the free surface.

The empirical breaking-wave model presented by [4] is implemented in REEF3D::FNPF. Both free surface conditions (2) and (3) are modified and extended by one extra element which mimics a spilling breaker and models energy dissipation similar to turbulent viscosity.

The additional elements of the free surface conditions is defined as:

$$\begin{aligned}\frac{\partial\eta}{\partial t} &= \ldots + \nu_B(x,t)\left(\frac{\partial^2\eta}{\partial x^2}\right)\\ \frac{\partial\widetilde{\Phi}}{\partial t} &= \ldots + \nu_B(x,t)\left(\frac{\partial^2\widetilde{\phi}}{\partial x^2}\right)\end{aligned} \tag{4}$$

where the so called wave-breaking turbulent viscosity $\nu_B(x,t)$ is given by

$$\nu_B(x,t) = \begin{cases}\nu_{B0}, & x \in D_b\\ 0, & \text{otherwise.}\end{cases} \tag{5}$$

D_b is the location where the dissipation is applied. Its location is defined by two parameters α and $SlopeB$ where $SlopeB = \partial\eta/\partial x$ is the front steepness of a wave and its value defines the limit when a wave will be identified as breaking in the potential solver and the value of α define the length of the damping zone (D_b) upwave (Figure 1).

The bottom boundary condition represents an impervious solid boundary:

$$\frac{\partial\Phi}{\partial z} + \frac{\partial h}{\partial x}\frac{\partial\Phi}{\partial x} + \frac{\partial h}{\partial y}\frac{\partial\Phi}{\partial y} = 0,\ \ z = -h. \tag{6}$$

where $h = h(\mathbf{x})$ is the water depth measured from the still water level to the seabed.

The Laplace equation with the boundary conditions is solved with a finite difference method on a σ-coordinate system. A σ-coordinate system deforms with the free surface and is also flexible in the handling of irregular boundaries. The relationship between a Cartesian grid and a σ-coordinate is as follows:

$$\sigma = \frac{z + h(\mathbf{x})}{\eta(\mathbf{x},t) + h(\mathbf{x})}. \tag{7}$$

The vertical grid stretching is defined with the help o the sinh function:

$$\tilde{\sigma} = 1 - \frac{\sinh(\delta(\sigma - 1))}{\sinh(-\delta)} \tag{8}$$

where σ is the uniform σ-coordinates, δ is the stretching factor and $\tilde{\sigma}$ is the new σ-coordinates. $\tilde{\sigma}$ will be referred as σ further in this paper. This stretching method is used in the simulations with uniform horizontal grid spacing. The grid is generated by REEF3D at the start of the simulation.

Once the velocity potential Φ is obtained in the σ-domain, the velocities can be calculated as follows:

$$u(\mathbf{x},z) = \frac{\partial\Phi(\mathbf{x},z)}{\partial x} = \frac{\partial\Phi(\mathbf{x},\sigma)}{\partial x} + \frac{\partial\sigma}{\partial x}\frac{\partial\Phi(\mathbf{x},\sigma)}{\partial\sigma}, \tag{9}$$

$$v(\mathbf{x},z) = \frac{\partial\Phi(\mathbf{x},z)}{\partial y} = \frac{\partial\Phi(\mathbf{x},\sigma)}{\partial y} + \frac{\partial\sigma}{\partial y}\frac{\partial\Phi(\mathbf{x},\sigma)}{\partial\sigma}, \tag{10}$$

$$w(\mathbf{x},z) = \frac{\partial\Phi(\mathbf{x},z)}{\partial z} = \frac{\partial\sigma}{\partial z}\frac{\partial\Phi(\mathbf{x},\sigma)}{\partial\sigma}. \tag{11}$$

Wave generation in the numerical wave tank is handled using a Neumann boundary condition. Here, the spatial derivatives of the velocity potential are prescribed according to the wave maker kinematics. The velocity potential at the boundary can then be calculated as follows:

$$\varphi_{i-1} = -u(x,z,t)\triangle x + \varphi_i \tag{12}$$

where $u(x,z,t)$ is the horizontal velocity of the wave maker. The wave maker motion is defined through a time series of the piston locations or the flap/flap angles. In this paper, the measured motion of the top of the wave maker is used to generate the waves. An active absorption method is used to mitigate wave reflection in the three-hour simulation.

The Laplace equation is discretized using a second-order central difference scheme and is solved using a parallelized geometric multigrid pre-conditioned conjugated gradient solver provided by Hypre [14].

The convection terms at the free-surface are discretized with the fifth-order Hamilton-Jacobi weighted essentially non-oscillatory (WENO) scheme [15]. A WENO discretization stencil is based on smoothness of three local ENO-stencils. The local stencil with the highest smoothness is assigned the highest weight and contributes the most significantly to the solution. The scheme is therefore capable of handling large gradients without instability.

For the time treatment, a third-order accurate TVD Runge-Kutta scheme [16] is used with a constant time step. The model is fully parallelized following the domain decomposition strategy. Ghost cells are used to exchange information between adjacent domains and are updated with the values from the neighboring processors using the Message Passing Interface (MPI).

EXPERIMENTAL DATA

The experiments were carried out in SINTEF/NTNU's small towing tank [17] and [18, 19]. Two types of wave makers are available: a single flap hinged wave maker and a piston type wave maker. The wave maker is capable of generating regular, irregular as well as various wave groups. At the other end of the tank is a beach, with an adjustable height depending on the water depth. The main dimensions of the towing tank are: length 28 m, breadth 2.5 m, water depth between 0 and 1.0 m (model scale).

In the focused wave packet study the flap type wave maker was used with sloping bottom. An idealized gently sloping bottom was modeled in the towing tank using a frame construction. The frame is covered by solid walls on both side and at the bottom (Figure 2a and 2b). The motion of the top of the wave maker flap is measured during the test. The angle of the flap with respect to the upright position is calculated from this time series according to the geometry shown in Figure 2c. In the CFD simulation, a right handed coordinate system $Oxyz$ with the xy-plane on the still water line is applied, the z-axis vertically upwards, and with the origin at the upright position of the wave maker.

Wave probe nr.	x [m]	y [m]
WP 16	0.00*	0.00
WP 03	4.75	0.00
WP 02	11.27	0.00
WP 04	11.66	0.00
WP 09	12.01	0.00
WP 07	12.95	0.00

TABLE 1: Position of the wave probe which is used in this paper; * in the model test attached to the flap

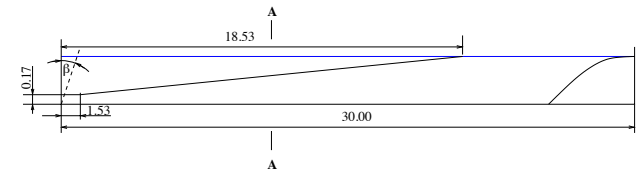

(a) Model setup with sloping bottom

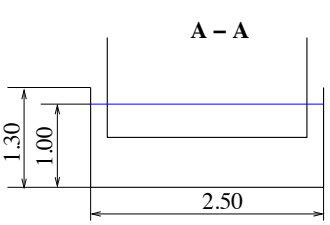

(b) Model setup with sloping bottom

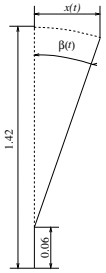

(c) Wave-maker geometry

FIGURE 2: Small towing tank with the model setup (All data are given in model scale.)

The wave propagates along the length of the tank in the positive x-direction. The position of the wave probes, which are compared with the numerical simulations, are defined in Table 1.

The piston type wave maker was used in the JONSWAP irregular sea state study with constant water depth based on considerations related to efficiency and parasitic waves. The parameters of the JONSWAP spectrum is given in Table 2 in model scale. The coordinate system is a right handed coordinate system, centred on the seabed at the mean position of the wave maker at the bottom of the tank. The positive x-axis points in the direction of wave propagation and the positive z-axis points upwards. All data given in this paper are given in model scale, both for the model tests and for the numerical simulations.

For the wave kinematics, the wave elevation was measured at 6 different distances, $x = 6.000, 10.000, 13.206, 15.281, 17.281, 19.281$m from the wave maker with a water depths of 0.54 m. Wave elevation was measured using resistive wave probes. The wave, piston position, temperature, and load signals were sampled at 200Hz (model scale) with Butterworth filter at 20Hz (model scale).

H_s [m]	T_p [s]	γ
0.16	1.41	5.0

TABLE 2: Main parameters of the sea state

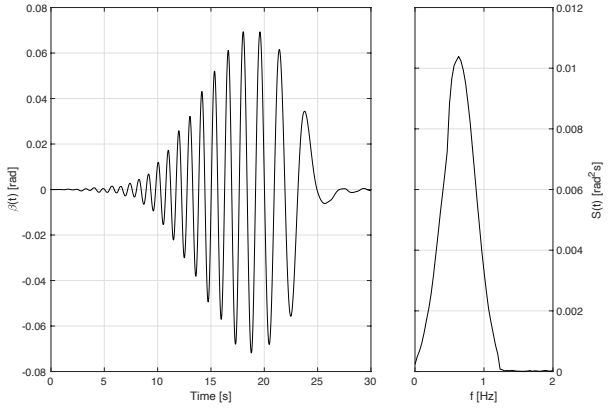

FIGURE 3: Estimated flap angle from the measured motion of the top of the wave maker

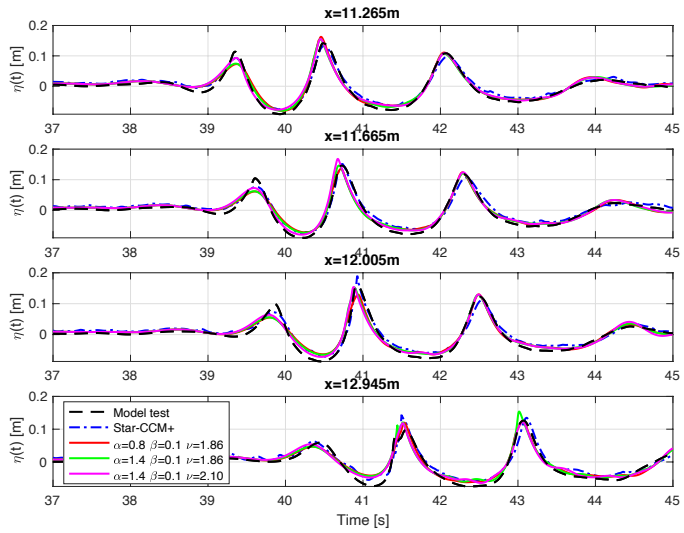

FIGURE 4: Estimated flap angle from the measured motion of the top of the wave maker

RESULTS

Breaking wave simulation

The numerical setup of the CFD simulation is described in detail in [1] and will not presented here. The numerical domain of the REEF3D::FNPF simulation is only extended to the end of the slope, 18.53m from the wave maker without any wave damping outlet condition. The slope is defined by REEF3D as a solids object in the numerical wave tank. The highest frequency of the wave maker motion is $f = 1.6$Hz (Figure 3) which gives the smallest wave period of $T = 0.625$s. The wave length of this wave is used to define the horizontal grid spacing dx of the REEF3D::FNPF simulation:

$$dx = \frac{\lambda}{35} = \frac{0.6\text{m}}{35} = 0.017\text{m}$$

. This gives 1100 horizontal grid points. The number of the vertical grid point is set to 11 with a stretching factor of $\delta = 2.25$ which defines 8 grid points in the vertical direction for the shortest wave length of 0.6 m. The shallow water wave phase velocity

Nr.	*slobeB* (α)	α (β)	ν_{B0}m^{2}s
1	0.8	0.1	1.86
2	1.4	0.1	1.86
3	1.4	0.1	2.10

TABLE 3: Parameter study of the wave breaking coefficients, the symbols in the parentheses are used in the diagrams

was used to estimate the constant time step for the simulation:

$$dt = \frac{dx}{c_{ph}} = \frac{dx}{\sqrt{hg}} = \frac{0.017\text{m}}{\sqrt{1\text{m}\ 9.81\text{m}^2/\text{s}}} = 0.0055\text{s}.$$

The calculation time is about 432 s on a 2010 MacPro with four processors. Three different wave breaking coefficient configurations are compared against the model test and CFD time series. The minimum wave slope (*SlopeB*) and the wave breaking turbulent viscosity ν_{B0} is varied (Table 3). The slope parameter defines the wave front steepness at which the wave breaking model is active. Increasing this value leads to the development of steeper waves in the potential theory based NWT.

The comparison of the time series at four locations is shown in Figure 4. At the closest location to the wave maker, $x = 11.265$ m one can observe that the weakest damping configuration nr. 1 gives slightly higher crest height at $t = 40.5$ s compared to all other time series. This trend cannot observed at other locations. One can not identify any trend or pattern in dependency of the wave breaking parameters. It is also expected because the wave breaking phenomena is sensitive to any small change in reality as observed in [20]. Therefore, a small change in the numerical parameter also has a large influence on the numerical waves. At the furthest location from the wave maker, at $x = 12.945$ m the wave is already broken in the model test at $t = 41.5$s. The CFD simulation underestimates the energy dissipation but laminar viscous mode was usedl in the simulation, which can explain this overestimation of the crest height. All of the potential theory based simulations survive the wave breaking and the crest height is reduced after the breaking due to the wave breaking

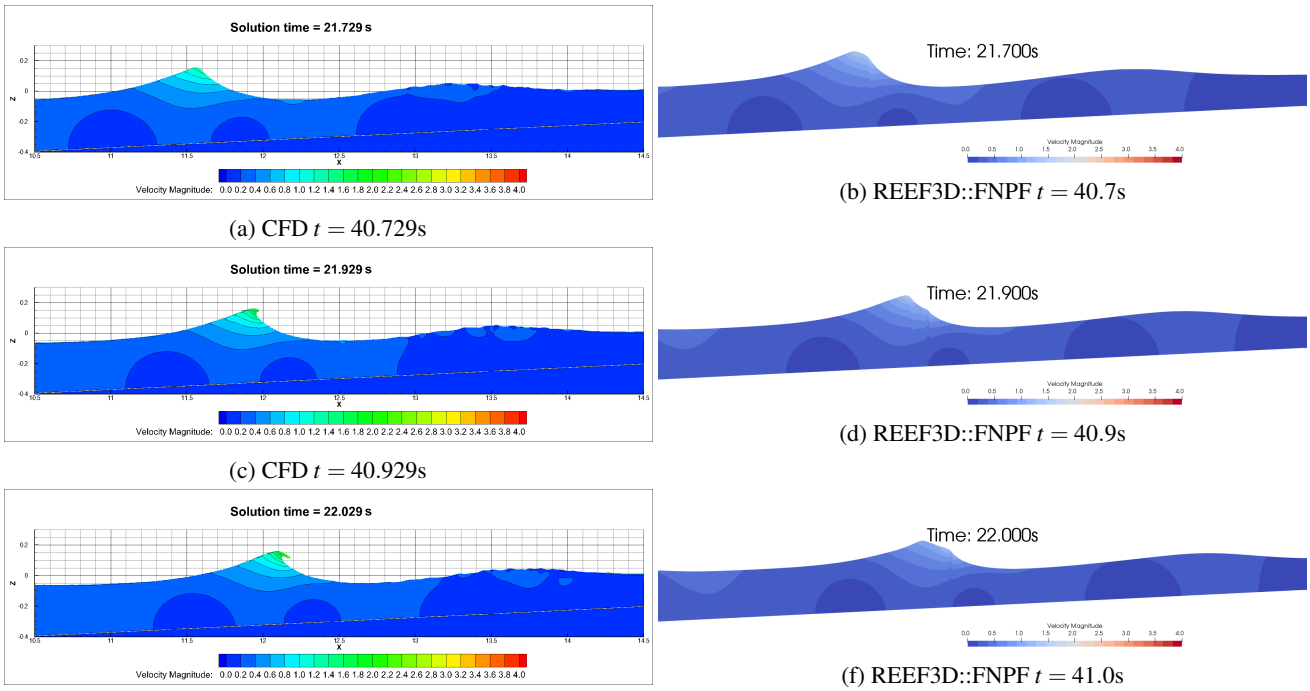

(a) CFD $t = 40.729$s

(b) REEF3D::FNPF $t = 40.7$s

(c) CFD $t = 40.929$s

(d) REEF3D::FNPF $t = 40.9$s

(e) CFD $t = 41.029$s

(f) REEF3D::FNPF $t = 41.0$s

FIGURE 5: Snapshots of the velocity magnitude [m/s]

model. All configurations give about the same wave crest height at time $t = 41.4$ s. However, the comparison of the next wave shows that configuration nr.3 gives the best agreement between the model test and the REEF3D::FNPF simulation. The comparison of the potential theory based results with the CFD results shows a larger degree of match between the time series than between any numerical simulation and model test data.

Comparison of the snapshots from the simulation in Figure 5 shows similar magnitude of velocity. The time is adapted to the CFD simulation but the caption shows the model test times in order to simplify the comparison between the snapshots and the time series shown in Figure 4. The REEF3D::FNPF snapshots are from the simulation with configuration nr. 3. The REEF3D snapshots also demonstrate the mode of action of the wave breaking model, the location and the length of D_b can be clearly identified on the lowest diagram. It is interesting to note that the configuration of the wave breaker model which is presented in [4] for the deep water spilling breaker is $SlopeB = 1.25$, $\alpha = 0.1$ and $\nu_{B0} = 1.86\text{m}^2\text{s}$ is close to the best identified configuration for shallow water overturning breaking wave. In the next section the standard configuration from [4] and the best configuration, nr. 3 are applied in the numerical simulation of a three-hour irregular sea state.

Three hours irregular sea-state simulation

The numerical setup of this simulation is presented in [21]. The results of the simulations will be presented in model scale in opposite to the above mentioned paper where all results are in full scale. The discussion of the results is mainly focussed on the effect of the parameters of the wave breaking model. A more detailed discussion of the results is presented in [21].

Three simulations with three different wave breaking configurations are carried out and their parameters are presented in Table 4. In the first configuration, the wave breaking turbulent viscosity ν_{B0} is set so low as possible as to not to crash the simulation. The second configuration is the "standard" setup and the third configuration is the best configuration as identified in the previous section.

The wave power spectrum, the crest height statistics are

Nr.	$slobeB\ (\alpha)$	$\alpha\ (\beta)$	$\nu_{B0}\text{m}^2\text{s}$
1	1.25	0.1	0.000125
2	1.25	0.1	1.86
3	1.40	0.1	2.10

TABLE 4: Parameter study of the wave breaking coefficients, the symbols in the parentheses are used in the diagrams

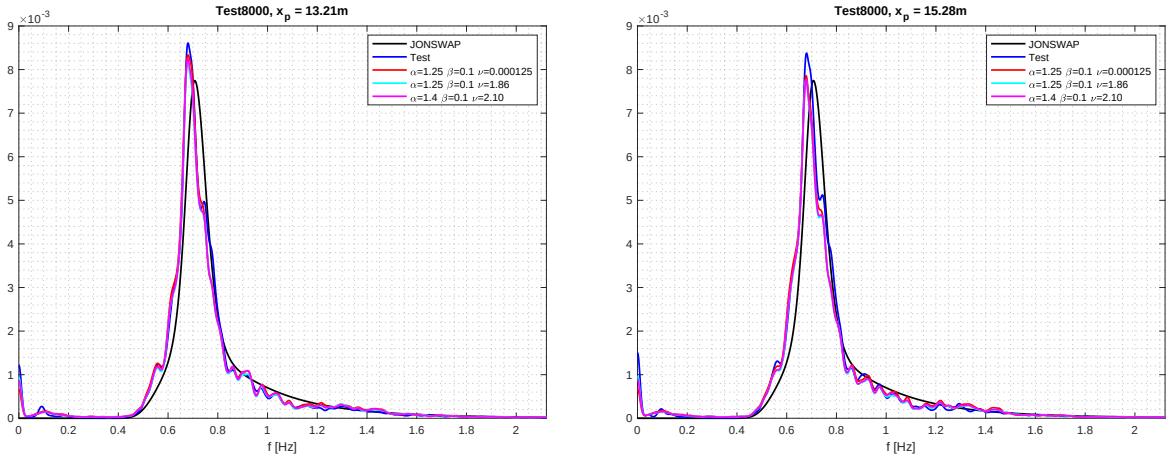

(a) $x = 13.21$m (b) $x = 15.28$m

FIGURE 6: Comparison of the wave power spectrum

compared against experimentally generated data, similar to that in the paper [4]. These analyses are applied at several locations. The most interesting location is at $x = 15.281$ m which is the location of a monopile structure. As mentioned earlier, the NWT simulation will be coupled to the CFD simulation. Therefore, the comparison of the sea statistics not only at the location of the monopile is interesting but the neighboring location upstream at $x = 13.206$ m because the velocity field around this position will be used to generate the waves in the CFD simulation. Bearing this in mind only the statistics at these two locations will be presented in this paper.

One can observe only small effect of the breaking wave model setup on the power spectrums at both locations. Mainly the energy at the peak period is slightly reduced due to the increased damping. The spectrum from the numerical simulations have better agreement with the spectrum from the model test at the upstream location.

The ensemble distribution of the crest heights is usually compared with the second-order Forristall distribution which is presented as a blue line in the diagrams of Figure 7. Huang & Zhang [22] give a formula defining the mean, the upper 99th and lower 99th percentiles of the wave crest heights. These formulae are based on a regression analysis of nonlinear numerical simulations with the JONSWAP spectrum with peak enchantment parameters γ between 1 and 4. These values are presented in green in the diagrams. At location $x = 13.21$ m the wave damping has no any effect on the largest wave event in the numerical simulations, all simulations over predict the crest height. However, one can clearly see a reduction of the crest height in the simulations with the larger damping for the wave events with crest heights under 0.15 m. Only the numerical simulation with the least damping gives a crest height distribution similar to the model test distribution. All other numerical simulations underestimate the wave crest height. This is not a trend. At the next location one can clearly see the effect of the wave damping. It is possible that at this location more waves are identified as breaking waves than at the upstream location. Without the damping, the numerical crest height distribution overshoots the model test curve for waves with crest heights larger than 0.12 m. The other simulations predict lower crest height distribution than the model test based distribution.

The largest effect of the wave breaking parameters can observed at the maximum elevation rise velocity $\partial\eta/\partial t$ in Figure 8 in the diagram at $x = 15.28$ m. Without damping, the large numerical waves are too steep while with damping they are too low on comparison with the experimental waves. At the other locations the steepness of the large numerical waves are in good agreement with the model test data, especially with the "standard" wave breaking setup.

It is important to mention, that one realization of a sea state is not enough to identify trends. It is necessary to run large number of seed number variations to establish a reliable data set for stochastic analysis. However, one can already identify that the representation of wave breaking in a potential theory based NWT has the largest effect on the maximum elevation rise velocity. Unfortunately, there does not exist any empirical or analytical distribution for these wave properties. Further, these values are calculated from the time derivative of the free surface elevation time series which are often noisy and it becomes necessary to use a filter. The filter setup can significantly change these values. In this study, we have not additionally filtered any time series of the free surface elevation.

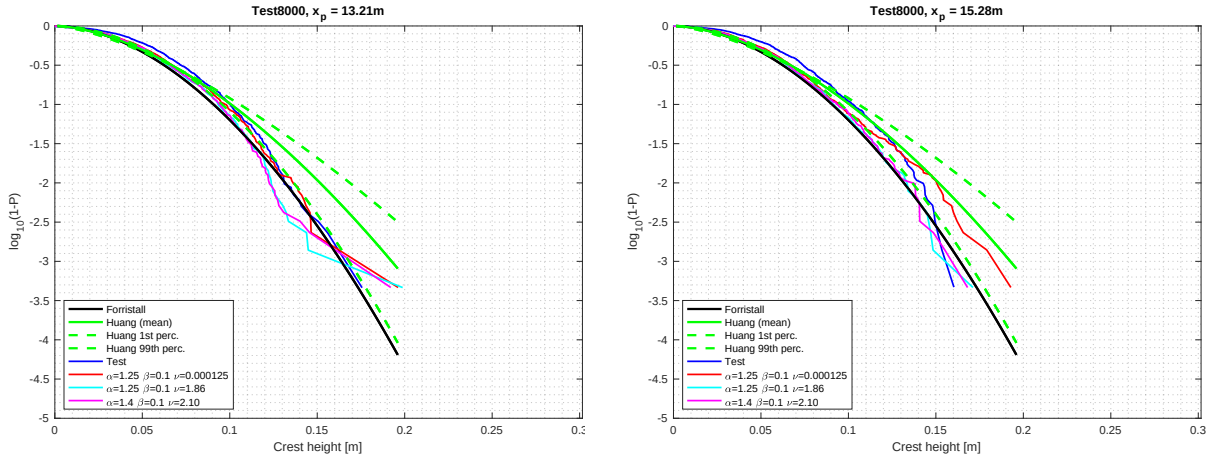

(a) $x = 13.21$m (b) $x = 15.28$m

FIGURE 7: Comparison of the three-hours ensembles of the crest heights

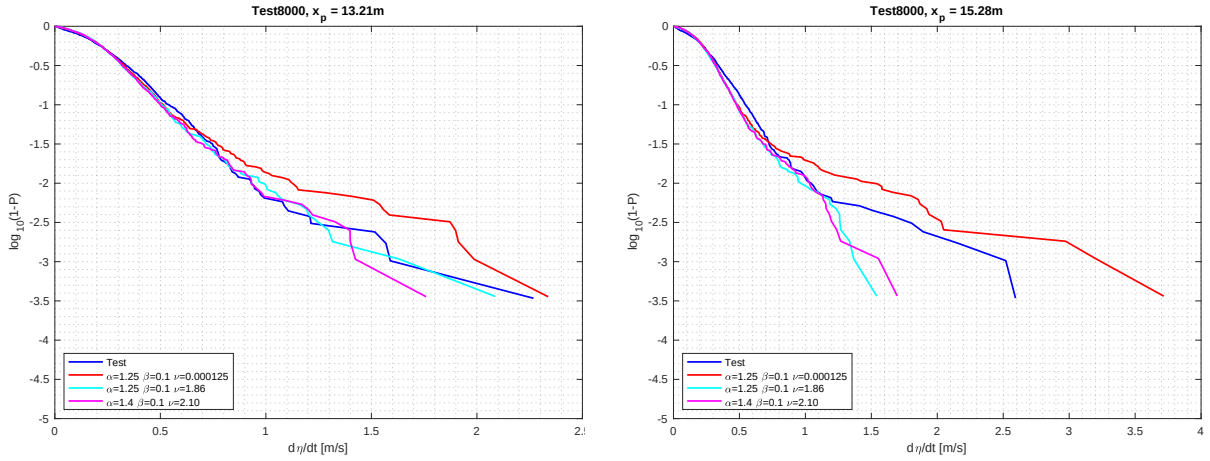

(a) $x = 13.21$m (b) $x = 15.28$m

FIGURE 8: Comparison of all three-hours ensembles of the maximum elevation rise velocity $\partial\eta/\partial t$

CONCLUSION

In this paper, the open-source hydrodynamic model REEF3D::FNPF is used to carry out simulations with breaking waves. The code was able to carry on the simulations without any crash demonstrating the robustness of the model.

Breaking waves generated in the facility at SINTEF Ocean/NTNU are simulated REEF3D::FNPF. The comparison of the simulations against CFD simulation show good agreement between the numerical models. Due to the chaotic nature of wave breaking, it was not possible to identify any trend even though the effect of the wave breaking parameter could be observed. It is interesting to note that the configuration of the wave breaker model which is presented in [4], [23] for the deep water spilling breaker can also work for a shallow water overturning breaking wave.

REEF3D::FNPF is used to carry out three-hour long simulations with the JONSWAP spectrum in intermediate water depth conditions in order to identify the influence of the breaking model parameters on the statistical properties of the generated waves and compared against model test data. The largest effect of the wave breaking parameters have are for the maximum elevation rise velocity $\partial\eta/\partial t$. The setup with the smallest damping might give a better but conservative numerical wave environment regarding to the largest waves. It is necessary to run a large number of seed number variations of the sea state to establish a reliable data set for stochastic analysis. Using coupled simulations for the largest wave events a better basis for comparison and better identification of the effect of the parameters of the wave breaking model can be established. This is planned for the next phase of the project.

ACKNOWLEDGMENT

The authors are grateful to the grants provided by the Research Council of Norway under WAS-XL project (No. 268182 and High Resolution Numerical Modeling for Flexible Fish Cage Structures).

REFERENCES

[1] Pakozdi, C. P., Kendon, T. E., and Stansberg, C. T., 2012. "A numerical study of a focused wave packet near the surf zone". In Proceedings of the ASME 2012 31th International Conference on Ocean, Offshore and Arctic Engineering. OMAE2012-83796.

[2] Hirt, C., and Nichols, B., 1981. "Volume of fluid (VOF) method for the dynamics of free boundaries". *Journal of Computational Physics,* ***39***(1), pp. 201 – 225.

[3] Osher, S., and Sethian, J. A., 1988. "Fronts propagating with curvature-dependent speed: Algorithms based on hamilton-jacobi formulations". *Journal of Computational Physics,* ***79***(1), pp. 12 – 49.

[4] Baquet, A., Kim, J., and Huang, Z., 2017. "Numerical modeling using cfd and potential wave theory for three-hour nonlinear irregular wave simulations". In ASME 2017 36th OMAE, no. OMAE2017-61090.

[5] Huang, Z., and Guo, Q., 2017. "Semi-empirical crest distribution of long-crested nonlinear waves of three-hour duration". In Proceedings of the 36th International Conference on Ocean, Offshore and Artic Engineering. OMAE2017-61226.

[6] Sharma, N., and Dean, R., 1981. "Second-order directional seas and associated wave forces". *Journal of the Society of Petroleum Engineering*, pp. 129–140.

[7] Marthinsen, T., and Winterstein, S., 1992. "On the skewness of random surface waves". *Proceedings of the Second International Offshore and Polar Engineering Conference (ISOPE),* ***III***, pp. 472–478.

[8] Clauss, G. F., Stempinski, F., Stück, R., and Schmittner, C. E., 2006. "Computational and experimental simulation of nonbreaking and breaking waves for the investigation of structural loads and motions". In ASME 2006 25th OMAE, no. OMAE2006-92238.

[9] Wang, W., Kamath, A., Pakozdi, C., and Bihs, H., 2019. "Investigation of focusing wave properties in a nume- rical wave tank with a fully nonlinear potential flow model". *Journal of Marine Science and Engineering, Journal of Marine Science and Engineering,* ***7***(375). Issue 10.

[10] Bihs, H., Wang, W., Pakozdi, C., and Kamath, A., 2020. "A flexible fully nonlinear potential flow solver". *Journal of Offshore Mechanics and Arctic Engineering,* ***accepted***.

[11] Pakozdi, C., Wang, W., and Bihs, H., 2019. "Validation of a high-performance computing nonlinear potential theory based numerical wave tank for wave structure interaction". In Coastal Structures 2019, T. S. Nils Goseberg, ed., Bundesanstalt fur Wasserbau.

[12] Moideen, R., Ranjan Behera, M., Kamath, A., and Bihs, H., 2019. "Effect of girder spacing and depth on the solitary wave impact on coastal bridge deck for different airgaps". *Journal of Marine Science and Engineering*.

[13] Bingham, H. B., and Zhang, H., 2007. "On the accuracy of finite-difference solutions for nonlinear water waves". *J Eng Math,* ***58***, pp. 211–228.

[14] Falgout, R. D., Jones, J. E., and Yang, U. M., 2006. "Conceptual interfaces in hypre". *Future Gener. Comput. Syst.,* ***22***(1-2), Jan., pp. 239–251.

[15] Guang-Shan, J., and Chi-Wang, S., 1996. "Efficient implementation of weighted eno schemes". *Journal of Computational Physics,* ***126***(1), pp. 202–228.

[16] Chi-Wang, S., and Stanley, O., 1988. "Efficient implementation of essentially non-oscillatory shock-capturing schemes". *Journal of Computational Physics,* ***77***(2), August, pp. 439–471.

[17] Svangstu, E., 2011. "An investigation of wave conditions and wave induced loads for design of wind turbine foundations at 15 -40m depth". Master's thesis, NTNU, Trondheim, Norway, June.

[18] Thys, M., 2019. Model test report: Wave kinematics and loads. Tech. Rep. OC2019 F-079, SINTEF Ocean.

[19] H. Dadmarzi, F., Thys, M., and Bachynski, E. E., 2019. "Validation of Hydrodynamic Loads on a Large-Diameter Monopile in Regular Waves". In International Conference on Offshore Mechanics and Arctic Engineering, Vol. Volume 7A: Ocean Engineering. V07AT06A060.

[20] Pakozdi, C., j. h. Visscher, Stansberg, C. T., and Fagertun, J. T., 2015. "Experimental investigation of global wave impact loads in steep random seas". In 25th Annual International Ocean and Polar Engineering Conference, no. 2015-TPC-1135.

[21] Pakozdi, C., Fouques, S., Thys, M., Kamath, A., Wang, W., Dadmarzi, F. H., Bachynski, E., and Bihs, H., 2020. "Validation of numerical wave tank simulations using reef3d with jonswap spectra in intermediate water depth". In Proceedings of the ASME 2020 39th International Conference on Ocean, Offshore and Arctic Engineering. OMAE2020-18298.

[22] Huang, J., and Zhang, Y., 2018. "Semi-empirical single realization and ensemble crest distributions of long crest nonlinear waves". In Proceedings of the 37th International Conference on Ocean, Offshore and Artic Engineering. OMAE2018-78192.

[23] Seiffert, B. R., Ducrozet, G., and Bonnefoy, F., 2017. "Simulation of breaking waves using the high-order spectral method with laboratory experiments: Wave-breaking onset". *Ocean Modelling,* ***119***, pp. 94 – 104.